

The Intrinsic Relationship Between Microstructure Evolution and Thermal Fatigue Behavior of a Single-Crystal Cobalt-Base Superalloy

Wei-Min Gui^{1,2} · Hong-Yu Zhang¹ · Min Yang³ · Tao Jin¹ · Xiao-Feng Sun¹ · Qi Zheng¹

Received: 13 July 2017/Revised: 13 August 2017/Published online: 6 September 2017
© The Chinese Society for Metals and Springer-Verlag GmbH Germany 2017

Abstract The intrinsic relationship between the microstructure evolution and thermal fatigue behavior of a single-crystal cobalt-base superalloy has been investigated. The thermal fatigue tests are performed cyclically between room temperature and 1050 °C using V-notch plate specimens. Three states of thermal fatigue specimens are selected: the as-cast, solutionized as well as aged states. The solution treatment is carried out at 1260 °C for 24 h, which results in the dissolution of most of interdendritic continuous primary carbides. The subsequent aging treatment is carried out at 1100 °C for 100 h after solution treatment, resulting in the precipitation of a profusion of chain- and point-like $M_{23}C_6$ carbides in the matrix. The results indicate that the heat treatment can improve the thermal fatigue properties of the alloy and the effect of the solution treatment is more prominent than that of the aging treatment. The coarse and continuously distributed primary carbides in the as-cast state are changed into small and discontinuous distribution by heat treatment, which is the dominant factor in the improvement of thermal fatigue property. Additionally, the effect of oxidation behavior during thermal fatigue test on the thermal fatigue behavior is also studied.

KEY WORDS: Cobalt-base superalloys; Heat treatment; Thermal fatigue; Carbide; Oxidation

1 Introduction

Cobalt-base superalloys are widely used for vanes and combustor sections in industrial and aircraft turbines because of their combined superior temperature capability, thermal fatigue and hot corrosion resistance. Carbide precipitation is the dominant strengthening mechanism for

cobalt-base superalloys [1–4]. When used as turbine components, cobalt-base superalloys are subjected to cyclic thermal stress caused by the temperature gradients occurring during start-up, thrust change and shutdown of aircraft engines. Repetition of such thermal stress results in thermal fatigue of the alloy [5–7].

Thermal fatigue is the primary failure mode in the application of cobalt-base superalloys and thus has received much attention. Studies have shown that primary coarse carbides and the grain boundaries act as crack initiation sites and crack propagation paths [5–10]. In order to improve the thermal fatigue resistance of cobalt-base superalloys, much effort has been made, such as reducing dendritic spacing or using directional solidification [10–12]. However, a few attempts have been made to explore the influence of heat treatment on the thermal fatigue properties of cobalt-base superalloys. It is well established that heat treatment can not only transform metastable carbides into stable carbides, but also refine the

Available online at <http://link.springer.com/journal/40195>.

✉ Qi Zheng
qzheng@imr.ac.cn

¹ Superalloys Division, Institute of Metal Research, Chinese Academy of Sciences, Shenyang 110016, China

² School of Materials Science and Engineering, University of Science and Technology of China, Hefei 230026, China

³ State Key Laboratory of Solidification Processing, Northwestern Polytechnical University, Xi'an 710072, China

morphology and distribution of the carbides [1, 4, 13–17]. It is therefore necessary to study the effect of carbide evolution induced by heat treatment on the thermal fatigue property of cobalt-base superalloys. Furthermore, in order to obtain a deeper insight into this relationship, the single-crystal technology is applied to eliminate the effects associated with grain boundaries in our work.

The purpose of this work is thus to investigate the intrinsic relationship between microstructure evolution and thermal fatigue behavior of a single-crystal cobalt-base superalloy. Crack initiation and propagation modes, as well as microstructure changes, are examined in detail, with the aim of understanding the features which influence the thermal fatigue resistance.

2 Experimental

The chemical composition of the test cobalt-base superalloy is listed in Table 1. The cast single-crystal specimens were prepared by means of the Bridgman method at a constant withdraw rate of 6 mm/min in a directional solidification vacuum furnace. Three representative alloy states were selected for this investigation: the as-cast, solutionized as well as aged. The solution treatment was carried out at 1260 °C for 24 h and then air-cooled. The aging treatment was performed at 1100 °C for 100 h, which was applied after solution treatment.

The specimen geometry for thermal fatigue is schematically shown in Fig. 1. Note that there is a pre-fabricated V-notch and the notch direction is parallel to the orientation of primary dendritic growth [001]. The thermal fatigue test was carried out on a self-made thermal fatigue testing machine. Each cycle of thermal fatigue test was heated quickly to 1050 °C and held for 6 min in a furnace with air atmosphere and then quenched in 25 °C water for 30 s. The peak temperature represents the expected application temperature in an aircraft gas-turbine engine. Inspections were made every 40 cycles up to 200 cycles and at 250 and 300 cycles. Three specimens for each condition were selected. When cracks were observed, the longest crack length from crack tip to the notch was measured on both surfaces by a JEOL JSM-5800 scanning electron microscopy (SEM), and the average value was taken as the crack length.

Table 1 Chemical composition of the test alloy (wt%)

Cr	Ni	W	C	Ta	Ti	Zr	Al	Co
25.5	10.7	7.81	0.42	0.34	0.19	0.16	0.97	Bal.

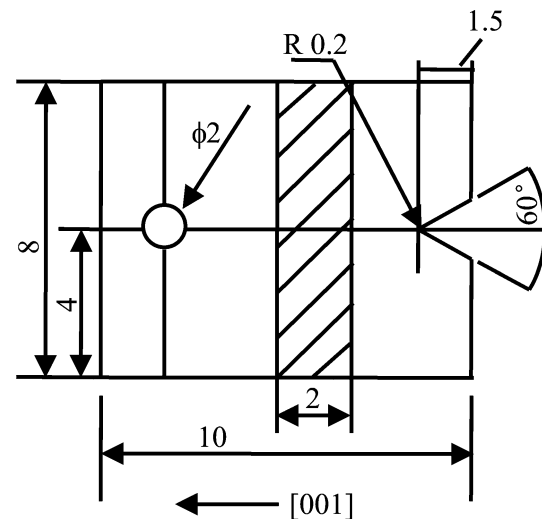


Fig. 1 Schematic diagram of the thermal fatigue specimen (mm)

The fracture surface and the microstructural evolution of fatigued specimens were examined by a Leica DM-400M optical microscope (OM) and SEM with back-scattered electron (BSE). The specimens for metallographic observation were etched electrolytically in a solution consisting of 42 pct H_3PO_4 + 34 pct H_2SO_4 + 24 pct H_2O for 10 s. Phase compositions were determined by energy-dispersive X-ray spectroscopy (EDS) and a Shimadzu electronic probe microanalysis (EPMA)-1610.

3 Results

3.1 Microstructures of Specimens Under Different States

The microstructures of the specimens under different states, the as-cast, solutionized and aged states, are given in Figs. 2 and 3. Figure 2 reveals that the carbides are mainly distributed in the interdendritic area. In addition, the carbides in the as-cast specimen are coarser and more continuous relative to the heat-treated specimens. As described in Ref. [17], the as-cast alloy consists of two types of primary carbides (Fig. 3a): network M_7C_3 and Chinese script MC . After solution treatment at 1260 °C for 24 h, the primary M_7C_3 decomposes into $M_{23}C_6$, and the formed $M_{23}C_6$ and primary MC mostly dissolve into the matrix (Fig. 3b). The subsequent aging treatment at 1100 °C for 100 h gives rise to a large amount of secondary $M_{23}C_6$ carbides in the matrix (Fig. 3c). In addition, the secondary $M_{23}C_6$ carbide is unevenly distributed and its morphology appears as point- and chain-like.

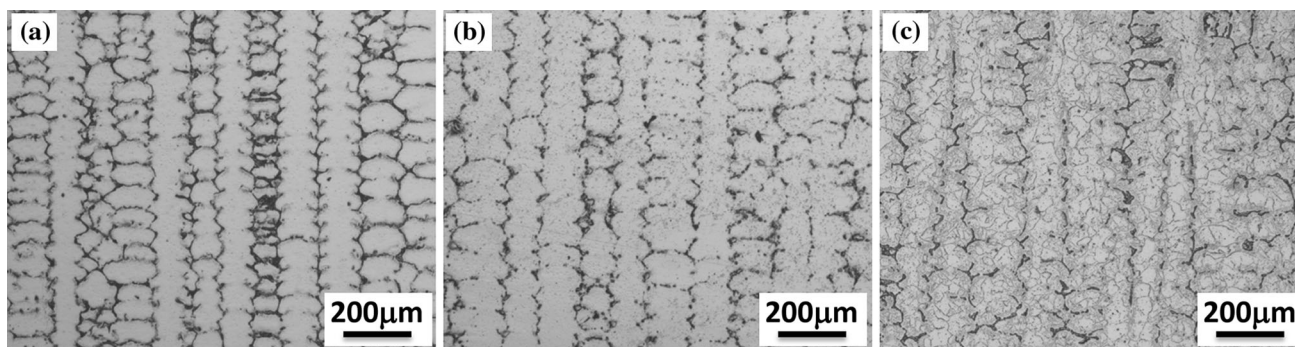


Fig. 2 Optical micrographs showing the dendritic structures of the three states of the specimens: **a** the as-cast, **b** solutionized, **c** aged

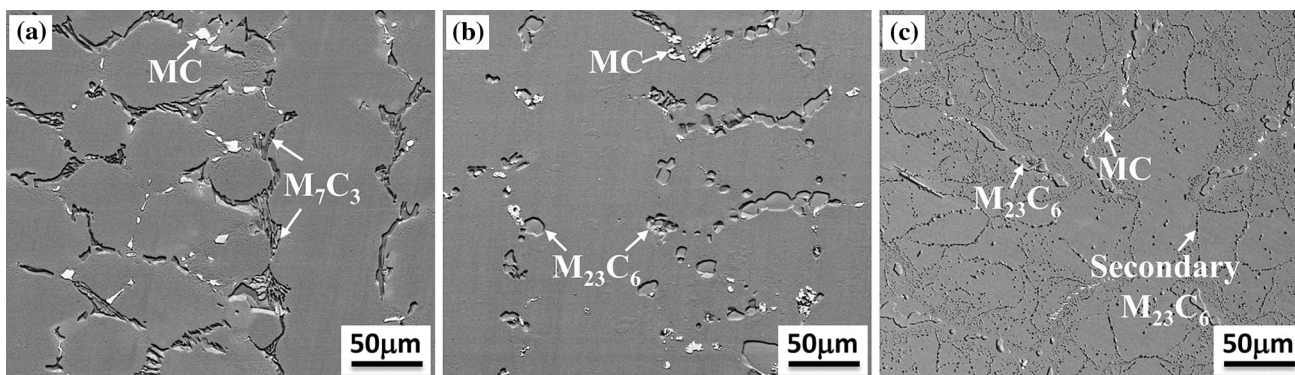


Fig. 3 SEM micrographs showing microstructures of the three states of the specimens: **a** the as-cast, **b** solutionized, **c** aged

3.2 Thermal Fatigue Life

Figure 4 gives the dependence of thermal fatigue crack length on the thermal fatigue cycles for the specimens at three states. It can be clearly seen that at the first 40 cycles, the crack lengths are nearly the same. With the increase in the cycles, however, the crack growth rates of the heat-treated specimens are slower than that of the as-cast

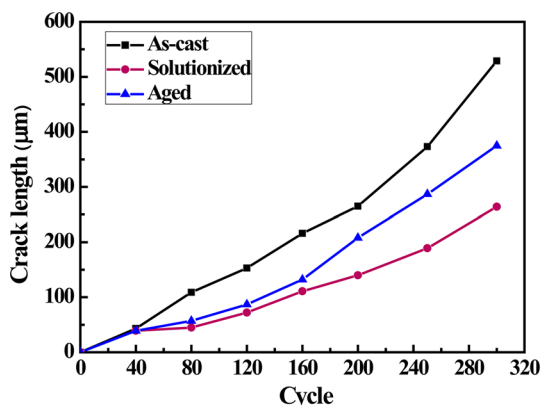


Fig. 4 Curves of the crack length as a function of cycle during thermal fatigue test for the specimens at the three states

specimen, especially the solutionized specimen. After 300 cycles, the crack length of the as-cast specimen is 25% longer than that of the aged specimen and is twice that of the solutionized specimen. This indicates that the thermal fatigue property of the alloy is improved by heat treatment, and the solution treatment is more significant.

3.3 Initiation and Propagation of Thermal Fatigue Cracks

A microstructural observation is performed on the specimens after thermal fatigue test with the aim to identify crack initiation and propagation. After the first 40 cycles, it can be observed that the cracks initiate at M_7C_3 in the as-cast specimen (Fig. 5a) and at $M_{23}C_6$ in the heat-treated specimens (Figs. 5b, c), and these carbides have been oxidized severely as well. In addition, it is noted that few cracks are found to initiate at MC carbides in these three states. With the increase in the cycles, the crack propagates forward, but the mode of crack propagation shows different characteristics at three states. After 160 cycles, it is seen that the cracks propagate mainly along the primary coarse and continuous carbides in the as-cast specimen (Fig. 6a). But in the solutionized specimen, the crack tip deflects

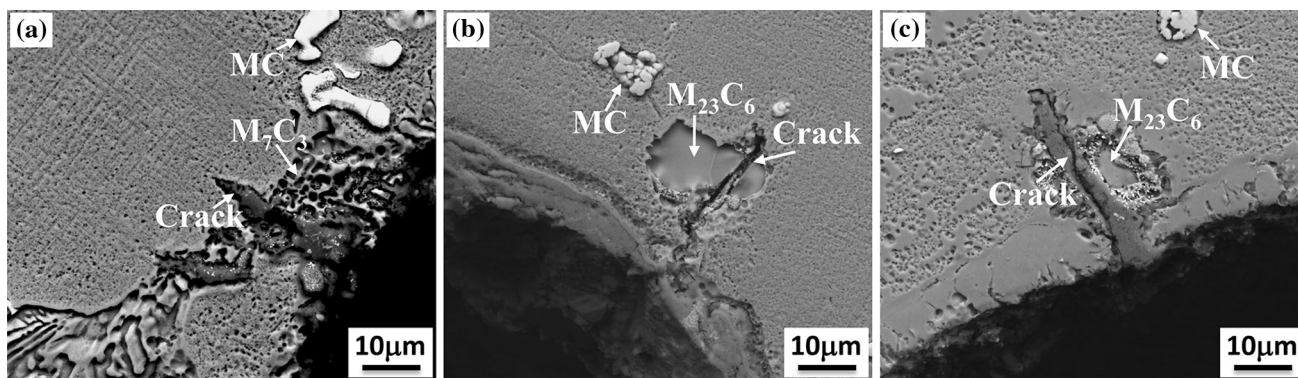


Fig. 5 Crack initiation in three-state specimens after 40 cycles: **a** the as-cast, **b** solutionized, **c** aged

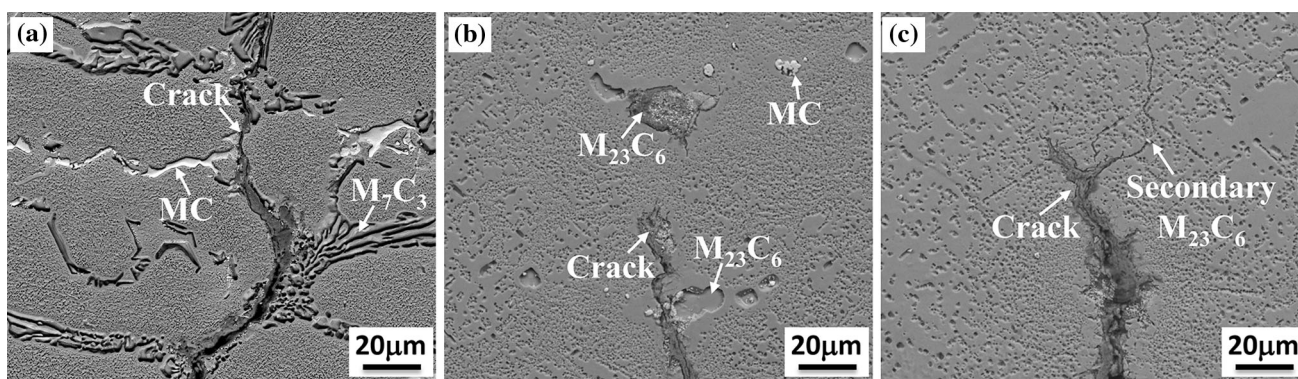


Fig. 6 Propagation morphologies near the crack tip in three-state specimens after 160 cycles: **a** the as-cast, **b** solutionized, **c** aged

from $M_{23}C_6$ carbide and enters the matrix, continuing to propagate in the matrix (Fig. 6b). In addition, it is found that the $M_{23}C_6$ carbides at the front of the crack tip have been already oxidized, which may create an easy path for crack propagation. Regarding the aged specimen, the crack tends to propagate along the chain-like secondary $M_{23}C_6$ carbide in the matrix as shown in Fig. 6c. Figure 7 shows the crack morphology after 300 cycles. It can be seen that the cracks propagate mainly along the interdendritic

regions or along the direction of 45° angle with the primary dendrites.

3.4 Oxidation Behavior

As described previously, the initiation and propagation of the cracks are strongly related to the oxidation. Hence, attention should be paid to the oxidation phenomena occurring during thermal fatigue in order to gain insight

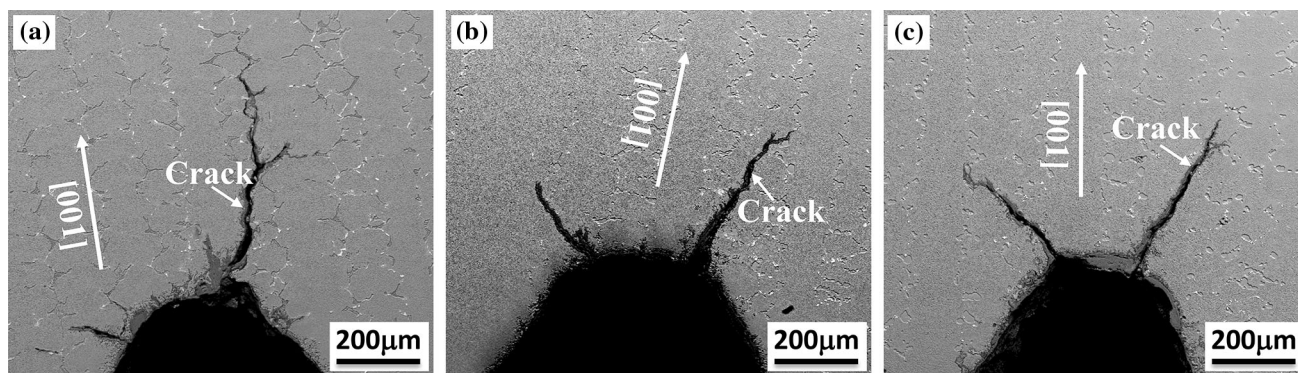


Fig. 7 Propagation morphologies of thermal fatigue cracks in three-state specimens after 300 cycles: **a** the as-cast, **b** solutionized, **c** aged

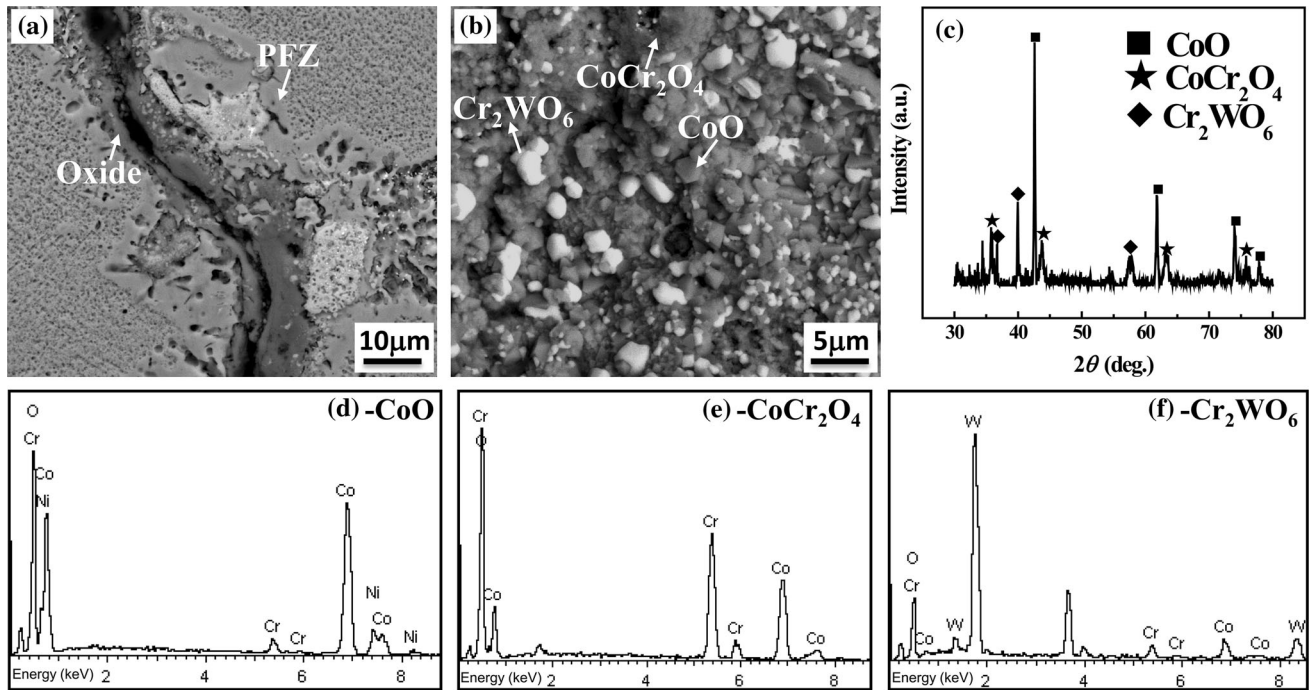


Fig. 8 Microstructures, XRD pattern and EDS results of the oxidation products in the as-cast specimen after 300 cycles: **a** BSE micrograph of the crack surface, **b** BSE micrograph of the fracture surface, **c** XRD pattern, **d–f** EDS results of CoO, CoCr₂O₄ and Cr₂WO₆, respectively

into the effect of oxidation on thermal fatigue behavior. In the as-cast specimen, it can be seen that the crack is filled with the mixture of white and gray phases from the higher-magnification image shown in Fig. 8a. In addition, the precipitate-free zone (PFZ) is found near the crack. From the fracture observation (Fig. 8b), three different structural forms coexist on the fracture surface after 300 cycles: the dark gray polygonal blocks, the light gray flocculent particles and the white round particles. The XRD result demonstrates that the microstructure on the fracture surface consists of three types of oxidation products, CoO, CoCr₂O₄ and Cr₂WO₆ (Fig. 8c). Combined with the EDS results (Fig. 8d–f), it can be confirmed that the Co-rich dark gray polygonal block is CoO, the Cr-rich light gray flocculent particle is CoCr₂O₄, and the W-rich white round particle is Cr₂WO₆. Similar observations of both solutionized and aged specimens show the presence of PFZ and the same type of oxidation products in the cracks (Fig. 9). However, it is clearly seen that the aged specimen has more oxides and PFZ regions with respect to the other two-state specimens.

EPMA area analysis is performed to investigate the degree of oxidation near the crack tip. The morphology near the crack tip of the as-cast specimen and the corresponding EPMA map of the distribution of O element are displayed in Fig. 9. The map scanning result of O element

reveals that M_7C_3 and MC carbides at the crack tip have been oxidized severely, but the matrix is barely oxidized.

4 Discussion

4.1 Effect of Carbide Microstructure on Thermal Fatigue Property

It is apparent from the above observations that the initiation and propagation of the thermal fatigue cracks are sensitive to the morphology and distribution of the carbides. The different initiation and propagation paths of thermal fatigue cracks for the three-state specimens are schematically illustrated in Fig. 11. During thermal fatigue test, thermal stress can be formed at the carbide/matrix interface due to the different thermal expansion coefficients [6, 7, 18, 19]. In addition, these carbides are hard and brittle. Therefore, the carbide crack easily occurs as a result of thermal stress. It is well established that the thermal expansion coefficient of matrix is $1.2 \times 10^{-5} \text{ }^\circ\text{C}^{-1}$, greater than that of M_7C_3 or $M_{23}C_6$ ($1.04 \times 10^{-5} \text{ }^\circ\text{C}^{-1}$), which is nearly twice as MC ($0.67 \times 10^{-5} \text{ }^\circ\text{C}^{-1}$) [20, 21]. Logically, crack initiation readily occurs at MC carbide rather than M_7C_3 or $M_{23}C_6$ carbide due to the difference in thermal expansion coefficients. However, it should be emphasized that the thermal fatigue test was carried out under the air atmosphere, and

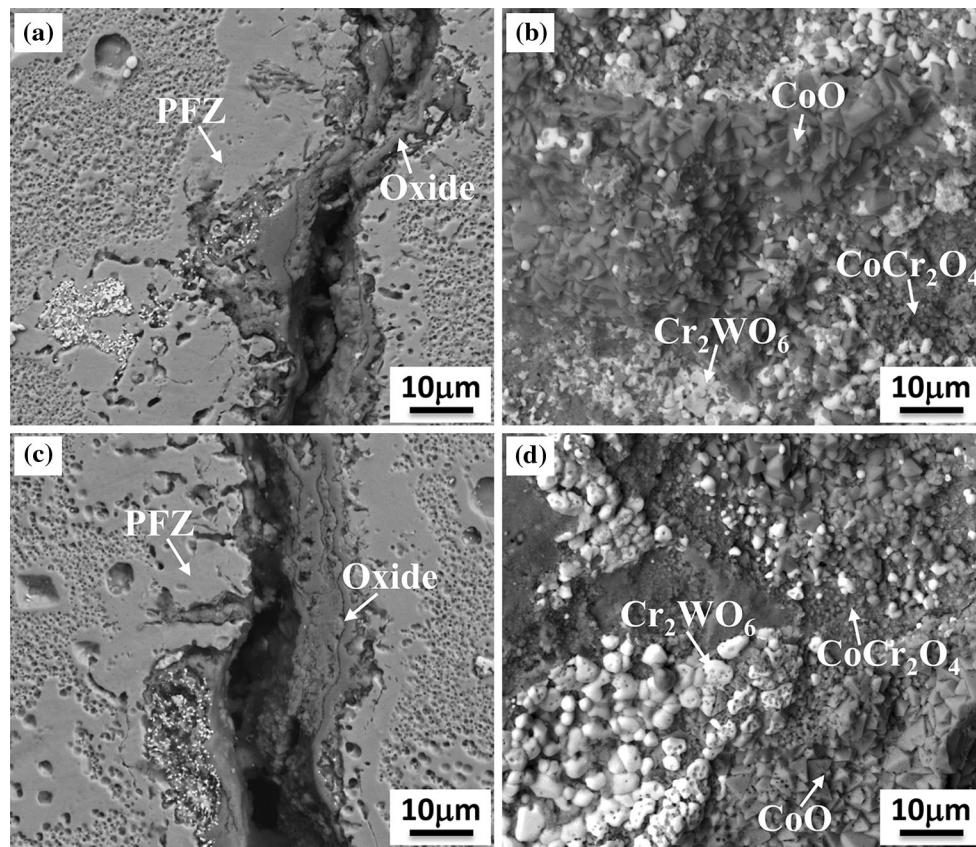


Fig. 9 Microstructures of crack surface and fracture surface in the solutionized and aged specimens after 300 cycles: **a, b** solutionized specimen, **c, d** aged specimen

the carbides can be oxidized at high temperature. It is known that M_7C_3 and $M_{23}C_6$ are rich in Cr, while MC is rich in Ta and Zr [17], and Cr is a more easily oxidizable element; thus, M_7C_3 and $M_{23}C_6$ carbide are more easily oxidized than MC carbide. Considerable evidences show that oxidation plays a major role in crack initiation. In MAR-M 509 cobalt-base superalloy, Reuchet and Remy [22] reported that the cracks were initiated at oxidized MC carbides in air and matrix/ MC interfaces in vacuum during high-temperature low-cycle fatigue. It is shown that air definitely alters the mechanism of crack initiation compared with the mechanism under vacuum. As a result, these oxidized M_7C_3 and $M_{23}C_6$ carbides are more likely to become potential crack nuclei than oxidized MC . Besides, it should be noted that the extrusions are caused by volume changes when the carbides are transformed to oxides. Thus, internal stresses are built up during oxide growth, which could superimpose on thermal stress. Furthermore, the fracture of the brittle oxide film occurs due to thermal stress (Fig. 8b), which provides the channel for oxygen entering into the crack and thus causes further oxidation at

the crack surface. Evidently, oxidation accelerates the crack initiation.

Thermal fatigue crack starts to propagate with the increase in cycles after crack initiation. After 40 cycles, the crack length of three specimens shows no significant difference due to less cycles. However, with the increase in the cycles, a clear difference appears in the crack growth rate for the three-state specimens. With regard to the as-cast specimen (Fig. 11a), the primary carbides in the interdendritic area are coarse and almost continuously distributed. These strong carbide alignments can effectively promote crack advance. Thus, when the crack passes through the broken M_7C_3 , it easily propagates along primary carbides (Fig. 6a). As a result, the crack propagation becomes faster after the first 40 cycles (Fig. 4). For the solutionized specimen (Fig. 11b), the solution treatment not only causes metastable M_7C_3 to decompose into stable $M_{23}C_6$ but also makes primary MC mostly dissolve into the matrix [17]. It is found that the primary metastable M_7C_3 in the as-cast specimen can keep its stability without the occurrence of phase transition during thermal fatigue process. This indicates that the more

stable $M_{23}C_6$ obtained by solution treatment is not the key for the better thermal fatigue property of the solutionized specimen. The main reason for this should be attributed to the changes in the size and distribution of carbides. The size of the carbides becomes smaller, and the carbide alignment has been broken in the solutionized specimen (Figs. 2b, 3b). This leads to that the crack cannot continue to propagate along the carbide alignment but in the matrix instead (Fig. 6b). The crack propagation performs slowly in the matrix since the matrix has good plasticity and can relieve stress concentration effectively. In addition, the matrix has better oxidation resistance than the carbides (Fig. 10b), which can reduce the effect of oxidation on crack propagation. Apart from these factors, the matrix is in the supersaturation state after solution treatment, which is favorable for the precipitation of uniformly dispersed $M_{23}C_6$ carbides. These secondary $M_{23}C_6$ carbides can hinder crack propagation during cycle fatigue [23]. Accordingly, the growth rate of the crack in the solutionized specimen is lower than that of the as-cast specimen especially during higher cycles (Fig. 4). Therefore, the solutionized specimen exhibits better thermal fatigue resistance than the as-cast specimen. From the experimental results, it is evident that the finer and discontinuously distributed carbides are the dominant factors to improve thermal fatigue resistance. In the case of the aged specimen (Fig. 11c), the first step of solution treatment makes primary carbides mostly dissolve into the matrix. Thus, the aged specimen has better thermal fatigue resistance than the as-cast specimen. After subsequent aging treatment at 1100 °C/100 h, a large number of secondary $M_{23}C_6$ carbides precipitate in the matrix. Nevertheless, it should be emphasized that some secondary $M_{23}C_6$ carbides present the chain morphology (Fig. 11c). These chain structures can provide preferred propagation paths for the crack during thermal fatigue process (Fig. 6c), which causes the increase in the crack growth rate. Furthermore,

the precipitation of Cr-rich $M_{23}C_6$ carbide by aging treatment has consumed a large amount of Cr element in the matrix, resulting in a decrease in the oxidation resistance of the matrix. Thus, it appears that more PFZ and oxides are produced around the crack as shown in Fig. 9c. Consequently, the brittle oxides are broken under thermal stress, making the crack easier propagate in the matrix. Therefore, the thermal fatigue resistance of the aged specimen is worse than that of the solutionized specimen. According to the above analysis, it suggests that the optimization of the microstructure of the carbides by heat treatment is an effective way to improve thermal fatigue property.

Besides, the direction of crack propagation appears along 45° to the primary dendrite orientation (Fig. 7c). The similar phenomenon is also observed in some directionally solidified nickel-base superalloys during cycle fatigue [24, 25]. Actually, it is related to the crystal structure of the alloy. The matrix of our alloy is a face-centered cubic structure; [011] (111) is an easy slip system. Along the direction of [011], the maximum shear stress is obtained [24]. Therefore, the crack propagates easily along these two directions.

4.2 Oxidation Behavior Associated with Thermal Fatigue

Previous studies on static oxidation of cobalt-base superalloys at high temperature have been done, like X-40 [26] and DZ40M [27] cobalt-base superalloys. The oxidation products reported in these studies are mainly CoO, Cr_2O_3 and $CoCr_2O_4$. In our study, the cracks are filled with oxidation products (Fig. 8), mainly CoO, $CoCr_2O_4$ and Cr_2WO_6 , which are different from those reported in Refs. [26, 27]. This might be related to different experimental temperatures and stress conditions. However, little research on the oxidation behavior that occurs during thermal fatigue has been reported until now. Therefore, the formation

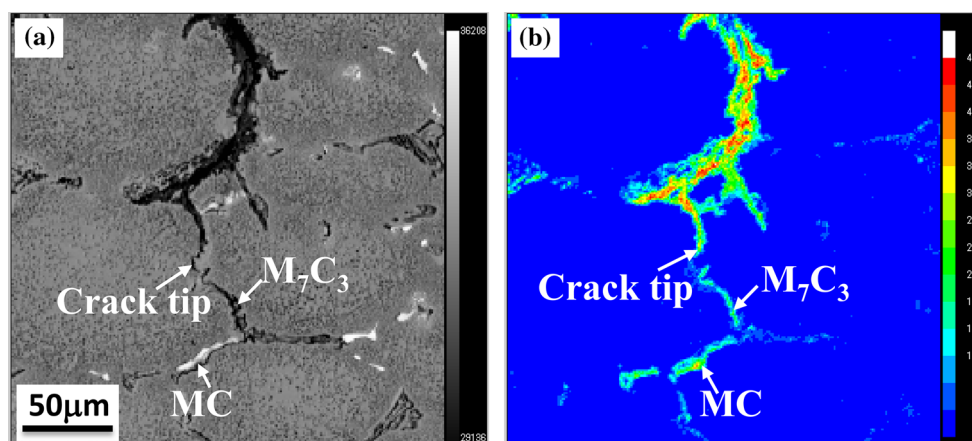


Fig. 10 a Morphology near the crack tip, b the corresponding EPMA map of the distribution of O element in the as-cast specimen

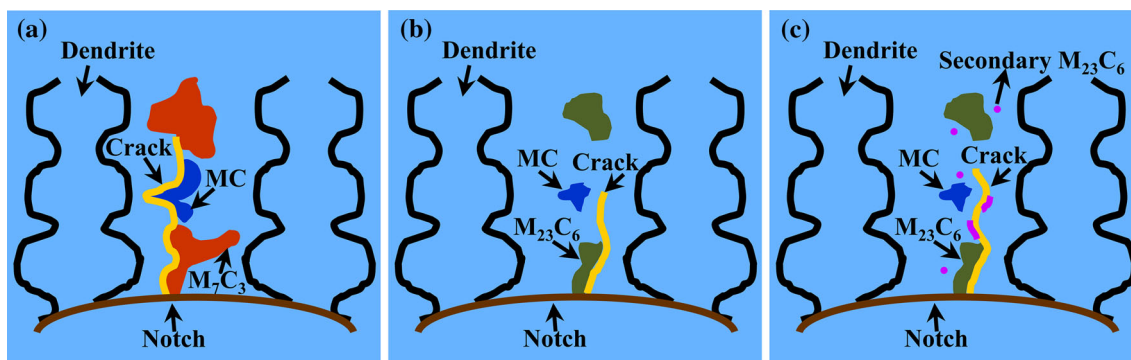


Fig. 11 Schematic illustration of the different initiation and propagation paths of thermal fatigue cracks for the three-state specimens: **a** the as-cast, **b** solutionized, **c** aged

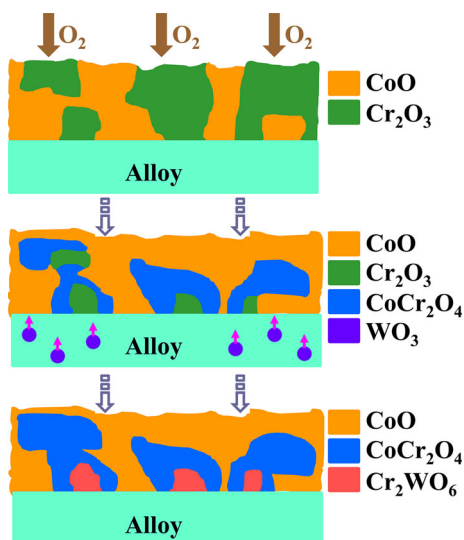


Fig. 12 Schematic diagram for the formation process of oxidation products in the crack

mechanism of the oxidation products in the crack should be analyzed in detail. Based on the experimental results, the formation mechanism of the oxidation products in the crack is proposed and schematically illustrated in Fig. 12. During the initial stages of thermal fatigue test, CoO and Cr₂O₃ form simultaneously. It has been established that the growth rate of CoO is faster than that of Cr₂O₃ [28]. As a result, it causes the overgrowth of the CoO layer and the presence of CoO in the outer oxide layer. Along with the oxidation process, the CoO becomes destabilized and reacts with Cr₂O₃ to form the thin spinel layer of CoCr₂O₄ [27]. In addition, oxide films break under thermal stress and the fresh metal is exposed to oxygen again. Thus, the W element in the matrix is also involved in the oxidation reactions, producing volatile WO₃ oxide. When the gaseous WO₃ meets Cr₂O₃, the reaction of WO₃ + Cr₂O₃ → Cr₂WO₆ occurs to form Cr₂WO₆ [29]. Accordingly, it can be inferred that Cr₂WO₆ is rarely observed in the static oxidation process due to the absence of thermal stress. As

the oxidation reaction continues, the Cr₂O₃ layer is gradually depleted and ultimately difficult to be detected in the oxidation production by XRD.

Furthermore, PFZ is observed along the crack in the alloy (Figs. 8a, 9a, c), which results from oxidation reactions. It has been known that the formation of oxidation products requires the consumption of Cr element in the matrix (Fig. 8d–f). Then, it inevitably causes the already precipitated Cr-rich secondary M₂₃C₆ near the crack to dissolve into the matrix to compensate for the consumption of Cr element. Accordingly, it results in the appearance of PFZ near the crack. This phenomenon is similar to the occurrence of γ' denuded zone near the crack during thermal fatigue in nickel-base superalloys [10, 30–32].

5 Conclusions

The present study focuses on the intrinsic relationship between the microstructure evolution and thermal fatigue behavior of a single-crystal cobalt-base superalloy. Main conclusions of this study can be drawn as follows:

1. The thermal fatigue property of the solutionized specimen is the best, the aged specimen is the second, and the as-cast specimen is the worst.
2. The improvement of thermal fatigue resistance results from the optimization of the size and distribution of the carbides by heat treatment, which effectively hinders the initiation and propagation of the cracks.
3. The initiation and propagation of the cracks are closely related to the oxidation. The crack is filled with oxidation products, mainly CoO, CoCr₂O₄ and Cr₂WO₆.

Acknowledgements This research was supported by the National Natural Science Foundation of China (Nos. 51331005, 51601192, 51671188 and 11332010) and the High Technology Research and

Development Program of China (No. 2014AA041701). Appreciation is expressed to Shuai Guan for helpful discussion.

References

- [1] C.T. Sims, N.S. Stoloff, W.C. Hagel (eds.), *Superalloys II* (Wiley, New York, 1987)
- [2] F.R. Morral, L. Habraken, D. Coutsouradis, J.M. Drapier, M. Urbain, *Met. Eng. Q.* **9**, 1 (1969)
- [3] C.P. Sullivan, J.D. Varin, M. Donachie, *Met. Eng. Q.* **9**, 16 (1969)
- [4] C.T. Sims, *J. Met.* **21**, 27 (1969)
- [5] F. Rezaei-Aria, M. Francois, L. Rémy, *Fatigue. Fract. Eng. Mater. Struct.* **11**, 277 (1988)
- [6] P.C. Xia, J.J. Yu, X.F. Sun, H.R. Guan, Z.Q. Hu, *Rare Metal. Mater. Eng.* **40**, 152 (2011)
- [7] M. Francois, L. Rémy, *Metall. Trans. A* **21**, 949 (1990)
- [8] C.G. Beck, A.T. Santhanam, *ASTM Spec. Tech. Publ.* **612**, 123 (1976)
- [9] P. Brauny, M. Hammerschmidt, M. Malik, *Mater. Sci. Technol.* **1**, 719 (1985)
- [10] D.A. Woodford, D.F. Mowbray, *Mater. Sci. Eng.* **16**, 5 (1974)
- [11] C.G. Beck, A.T. Santhanam, *Scr. Metall.* **12**, 255 (1978)
- [12] W.J. Molloy, *Adv. Mater. Proc.* **138**, 23 (1990)
- [13] W.H. Jiang, H.R. Guan, Z.Q. Hu, *Mater. Sci. Eng., A* **271**, 101 (1999)
- [14] A.M. Beltran, C.T. Sims, N.T. Wagenheim, *J. Met.* **21**, 39 (1969)
- [15] S. Hamar-Thibault, M. Durand-Charre, B. Andries, *Metall. Trans. A* **13**, 545 (1982)
- [16] J.R. Lane, N.J. Grant, *Trans. ASM* **44**, 113 (1952)
- [17] W.M. Gui, H.Y. Zhang, M. Yang, T. Jin, X.F. Sun, Q. Zheng, *J. Alloys Compd.* **695**, 1271 (2017)
- [18] Z.D. Fan, D. Wang, L.H. Lou, *Acta Metall. Sin. (Engl. Lett.)* **28**, 152 (2015)
- [19] Z.J. Zhou, D.Q. Yu, L. Wang, L.H. Lou, *Acta Metall. Sin. (Engl. Lett.)* **30**, 185 (2017)
- [20] H.O. Pierson, *Handbook of Refractory Carbides & Nitrides: Properties, Characteristics, Processing and Applications* (Noyes Publications, Bracknell, 1996)
- [21] W.F. Gale, T.C. Totemeir, *Smithells Metals Reference Book*, 8th edn. (Elsevier Butterworth Heinemann, Oxford, 2004)
- [22] J. Reuchet, L. Remy, *Mater. Sci. Eng.* **58**, 19 (1983)
- [23] W.H. Jiang, X.D. Yao, H.R. Guan, Z.Q. Hu, *J. Mater. Sci.* **34**, 2859 (1999)
- [24] J.H. Zhang, Y.J. Tang, Y. Yu, J.S. Zhang, Z.Q. Hu, *Acta Metall. Sin.* **24**, 254 (1988). (in Chinese)
- [25] X. Xiao, H. Xu, X.Z. Qin, Y.A. Guo, J.T. Guo, L.Z. Zhou, *Acta Metall. Sin. (in Chinese)* **47**, 1129 (2011)
- [26] C.A. Barrett, J.R. Johnston, W.A. Sanders, *Oxid. Met.* **12**, 343 (1978)
- [27] P.S. Liu, K.M. Liang, *Oxid. Met.* **53**, 351 (2000)
- [28] F.R. Morral, *Corrosion* **25**, 307 (1969)
- [29] N.S. Saleh, *J. Phys. C: Solid State Phys.* **17**, 3087 (1984)
- [30] M. Mansuri, S.M. Hadavi, K. Zangeneh-Madar, H. Abaszade, E. Zare, S. Hejazi, *Int. J. Mater. Res.* **105**, 1123 (2014)
- [31] M. Mansuri, S.M.M. Hadavi, E. Zare, M.M. Nabi, *Surf. Eng.* **32**, 201 (2016)
- [32] P.C. Xia, L. Yang, J.J. Yu, X.F. Sun, H.R. Guan, Z.Q. Hu, *Rare Metal.* **30**, 477 (2011)